Brief Communication

MOLECULAR METABOLISM

PAT2 regulates vATPase assembly and lysosomal acidification in brown adipocytes

Jiefu Wang [1,2,1], Yasuhiro Onogi [1,2,1], Martin Krueger [3], Josef Oeckl [4], Ruth Karlina [1,2], Inderjeet Singh [1,2], Stefanie M. Hauck [2,5], Regina Feederle [2,6], Yongguo Li [4], Siegfried Ussar [1,2,7,*]

ABSTRACT

Objective: Brown adipocytes play a key role in maintaining body temperature as well as glucose and lipid homeostasis. However, brown adipocytes need to adapt their thermogenic activity and substrate utilization to changes in nutrient availability. Amongst the multiple factors influencing brown adipocyte activity, autophagy is an important regulatory element of thermogenic capacity and activity. Nevertheless, a specific sensing mechanism of extracellular amino acid availability linking autophagy to nutrient availability in brown adipocytes is unknown.

Methods: To characterize the role of the amino acid transporter PAT2/SLC36A2 in brown adipocytes, loss or gain of function of PAT2 were studied with respect to differentiation, subcellular localization, lysosomal activity and autophagy. Activity of vATPase was evaluated by quenching of EGFP fused to LC3 or FITC-dextran loaded lysosomes in brown adipocytes upon amino acid starvation, whereas the effect of PAT2 on assembly of the vATPase was investigated by Native-PAGE.

Results: We show that PAT2 translocates from the plasma membrane to the lysosome in response to amino acid withdrawal. Loss or over-expression of PAT2 impair lysosomal acidification and starvation-induced S6K re-phosphorylation, as PAT2 facilitates the assembly of the lysosomal vATPase, by recruitment of the cytoplasmic V1 subunit to the lysosome.

Conclusions: PAT2 is an important sensor of extracellular amino acids and regulator of lysosomal acidification in brown adipocytes.

Keywords Brown adipocytes; Lysosomal acidification; Proton-coupled amino acid transporter; Transporter translocation across membranes; V-ATPase assembly

1. INTRODUCTION

Brown adipocytes, with their unique ability to dissipate excessive energy in form of heat through mitochondrial uncoupling, play an important role in regulating energy expenditure, as well as glucose and lipid homeostasis [1—3]. Importantly, brown adipocyte activity itself is tightly regulated by environmental signals, as well as the metabolic state of the organism [4—12]. This underscores the important role of brown adipocytes as rheostat sensing the organismal state to regulate whole body metabolic function through a complex network of neuronal, endocrine and nutritional inputs.

The role of the sympathetic nervous system, as well as glucose, fatty acids and other metabolites have been extensively described in the regulation of brown adipocyte activity [4—6,13,14]. However, surprisingly little is known about the potential role of amino acids in the regulation of brown adipocyte function. Alanine inhibits glucose oxidation of brown adipocytes [15], whereas leucine as well as arginine promote BAT growth and function [16,17].

Cellular amino acid levels are sensed and regulated by a complex network of proteins in and around the lysosome centered around mTORC1 activity [18]. Conditional ablation of raptor, an essential protein for mTORC1 activity, in adipocytes results in increased lipolysis and lipophagy, which is rescued by inhibition of autophagy through depletion of ATG7 [19]. In line with this, autophagy regulates adipocyte differentiation, thermogenic gene expression and brown fat activity [20,21]. Autophagy mediates degradation of various intracellular components through their delivery to the lysosome [22—24]. Thus, the lysosome governs intracellular lipid and amino acid availability and can modulate energy metabolism in brown adipocytes [25,26].

A central element for the proteolytic activity of the lysosome is vATPase-dependent luminal acidification [27]. vATPase activity itself is primarily regulated via its assembly, through the recruitment of the

[1]RG Adipocytes & Metabolism, Institute for Diabetes & Obesity, Helmholtz Diabetes Center, Helmholtz Zentrum München, German Research Center for Environmental Health GmbH, 85764, Neuherberg, Germany [2]German Center for Diabetes Research (DZD), 85764, Neuherberg, Germany [3]Institute for Anatomy, University of Leipzig, 04103, Leipzig, Germany [4]Chair for Molecular Nutritional Medicine TUM School for Life Sciences,Technical University Munich, Munich, Germany [5]Research Unit Protein Science, Helmholtz Zentrum München, German Research Center for Environmental Health GmbH, Neuherberg, Germany [6]Monoclonal Antibody Core Facility, Institute for Diabetes & Obesity, Helmholtz Diabetes Center, Helmholtz Zentrum München, German Research Center for Environmental Health GmbH, 85764, Neuherberg, Germany [7]Department of Medicine, Technische Universität München, Munich, Germany

[1] Jiefu Wang and Yasuhiro Onogi contributed equally to this work.

*Corresponding author. RG Adipocytes & Metabolism, Institute for Diabetes and Obesity, Helmholtz Center Munich, Ingolstaedter Landstrasse 1, 85764 Neuherberg, Germany. Tel.: +49 89 3187 2047. E-mail: siegfried.ussar@helmholtz-munich.de (S. Ussar).

Received April 8, 2022 • Accepted April 26, 2022 • Available online 2 May 2022

https://doi.org/10.1016/j.molmet.2022.101508

Abbreviations

AA	amino acid
ATG	autophagy-related gene
A.U.	arbitrary unit
BAT	brown adipose tissue
CBB	Coomassie Brilliant Blue
CD	chow diet
FCCP	Carbonyl cyanide-p-trifluoromethoxyphenylhydrazone
Con A	concanamycin A
IB	immunoblot
IBMX	3-isobutyl-1-methylxanthine
IP	immunoprecipitation
mTORC	mechanistic target of rapamycin complex
OCR	Oxygen consumption rate
PAT	proton-coupled amino acid receptor
PGF	perigonadal fat
PPARγ	peroxisome proliferator-activated receptor γ
SCF	subcutaneous fat
TA	tibialis anterior
UCP1	uncoupling protein 1

cytosolic V1 subunit to the membrane anchored V0 subunit during the maturation from the late endosome to the lysosome [28]. We previously identified the proton-coupled amino acid transporter PAT2/SLC36A2 as highly enriched in brown adipocytes [29]. However, in contrast to other brown adipocyte enriched genes, PAT2 expression was not regulated by chronic cold exposure or CL-316243 treatment and only slightly downregulated in BAT of db/db mice compared to db/+ controls [29]. PAT2 is a proton-coupled amino acid transporter that belongs to the SLC36 family [30,31], with very narrow substrate specificity [32] and strong pH dependence [32–35]. We showed that in contrast to the constitutive lysosomal amino acid transporter PAT1, PAT2 localizes to the plasma membrane of fully differentiated brown adipocytes [29]. However, the function of PAT2 in brown adipocytes is not known. Here we show that PAT2 resides at the cell surface of mature brown adipocytes and responds to changes in extracellular amino acid levels, as depletion of extracellular amino acids results in rapid translocation of PAT2 from the cell surface to the lysosome. We demonstrate that PAT2 interacts with and recruits the V1 domain of the vATPase to the lysosome, facilitating full assembly of the enzyme. Deregulation of PAT2 by either overexpression or knockdown results in hyper- or hypo-acidification of the lysosome, respectively, with profound effects on autolysosome formation and activation of mTORC1. Together, PAT2 serves as an amino acid sensor orchestrating intracellular organelle functions in brown adipocytes.

2. MATERIALS AND METHODS

2.1. Cell culture

For all experiments, a previously established murine brown preadipocyte cell line, derived from heterogeneous stromal vascular cells in BAT of an 8 week-old C57BL/6 mouse was used, cultured and differentiated as previously described [48]. To establish a PAT2 knockdown cell line, a shPAT2 (targeting sequence: CCGGCAGACTGAACAAGCCTTTCATCTCGAGATGAAAGGCTTGTTCAGTCTGTTTTTG) and its scrambled control shRNA (shScr), cloned into a pLKO.1-puro vector were purchased from Sigma Aldrich. PAT2 cDNA containing a HA-tag directly in front of the stop codon was cloned into the pCDH-CMV-puro plasmid to generate the PAT2-HA overexpression cell line. All plasmids were packed in lentiviruses (Cell Biolabs, VPK-205), concentrated using PEG-it (System Bioscience, SBI-LV810A-1) and preadipocytes were infected in presence of 9 μg/mL polybrene. Cells were cultured in medium containing DMEM (Thermo Fisher Scientific, 35050038), 10% fetal bovine serum, 1% penicillin-streptomycin (Thermo Fisher Scientific, 5000956) and 2.5 μg/mL puromycin (Cayman Chemical, Cay13884-500).

2.1.1. Adipocyte differentiation and amino acid starvation

Preadipocytes were grown to 100% confluence and the differentiation was induced with 0.5 mM IBMX (Sigma Aldrich, I5879), 5 μM dexamethasone (Sigma Aldrich, D1756), 0.125 mM indomethacin (Santa Cruz Biotechnology, sc-200503), 1 nM triiodothyronine (T3, Merck Millipore, 64245), 100 nM insulin (Sigma Aldrich, I9278) and 1 nM rosiglitazone (Santa Cruz Biotechnology, sc-202795). After two days, the medium was changed to medium containing only 100 nM insulin, 1 nM T3 and 1 nM rosiglitazone. The medium was changed every 2 days until day 8. For amino acid starvation, cells were washed twice with PBS (Thermo Fisher Scientific, 5001223) and cultured with amino acid free DMEM (GENAXXON bioscience, C4150.0500) containing 1% penicillin-streptomycin and dialyzed FBS (Thermo Fisher Scientific, A3382001) if indicated. Amino acid restimulation was performed by adding MEM Amino Acids solution (50X, Sigma Aldrich, M5550).

2.1.2. Transient transfection

Thirty microliter DMEM, 20 μL Polyfect (Qiagen, 301107) and 1 μg plasmid were incubated for 5 min and the transfection mix was dropped to cover all cells without medium. After 4 h incubation, cell culture medium was added.

2.2. Mouse experiments

Male C57BL/6N-Rj mice were purchased from Janvier and housed under 45–65% humidity and a 12h light: 12 h dark cycle at ambient temperature 22 ± 2 °C. For the fasting experiments, mice were transferred at the beginning of the dark cycle to a new cage without food but ad libitum access to water for 12 h. Animal experiments were conducted in accordance with the German animal welfare law and performed with permission and in accordance with all relevant guidelines and regulations of the district government of Upper Bavaria (Bavaria, Germany), ROB-55.2-2532.Vet_02-16-52.

2.3. Oil Red O staining

Cells were fixed with 10% formalin (Carl Roth, 4979.1) in PBS for 10 min, washed with PBS twice and incubated with 60% isopropanol for 5 min. Cells were incubated in 21% Oil Red O (Sima Aldrich, O0625) in 60% isopropanol for 10 min followed by four-time washing with distilled water. Images were taken using an EVOS XL Core Cell Imaging System (Thermo Fisher Scientific). Oil Red O was extracted by 100% isopropanol and quantified at 505 nm.

2.4. Western blot and co-immunoprecipitation

Cells or tissues were lysed in ice-cold RIPA buffer (50 mM Tris–HCl pH 7.4, 150 mM NaCl, 1 mM EDTA, 1% Triton X-100) containing 1% protease and phosphatase inhibitor cocktails (Sigma Aldrich, P8340; P5726 and P0044) on ice. After collection of lysate removed debris by centrifugation, protein concentrations were measured by BCA assay (Thermo Fisher Scientific, 10741395). Protein samples were mixed with NuPAGE™ LDS Sample Buffer (Thermo Fisher Scientific, NP0008) and incubated at 70°C for 10 min. Proteins were transferred to 0.45 μm PVDF membranes (Merck Millipore,

ISEQ00010), and blocked with 5% skim milk (Biomol, S1013-90A.500) in 10 mM Tris TBS-0.1% Tween 20 (TBST) for at least 1 h. Primary and HRP conjugated secondary antibodies (Table S1) were diluted in 5% BSA (Carl Roth, T844.2) or 5% skim milk in TBST. Amersham Hyperfilm ECL (GE, GE28-9068-36) and HRP substrate ECL (Merck Millipore, WBKLS0500) were used to detect signals. Band intensities were quantified by ImageJ.

2.4.1. Co-immunoprecipitation

Cells were lysed in Pierce IP Lysis Buffer (25 mM Tris—HCl pH 7.4, 150 mM NaCl, 1% NP-40, 1 mM EDTA, 5% glycerol) (Thermo Fisher Scientific, 87787) containing 1% protease and phosphatase inhibitors on ice and protein concentration was measured by BCA. One milligram of protein lysate was incubated with 1 μg anti-HA antibody (Table S1) overnight at 4°C. Ten microliter protein A/G agarose beads (Santa Cruz Biotechnology, sc-2003) were added to the lysate for 1 h at 4 °C. The beads were precipitated by centrifugation at 1,000×*g* at 4 °C for 3 min. Lysis buffer was used to wash beads 3 times and proteins were eluted with 2 × NuPAGE™ LDS Sample Buffer with 5% β-mercaptoethanol (Sigma Aldrich, M3148) at 70 °C for 5min and analyzed by western blot.

2.5. Blue native-PAGE

The NativePAGE Novex Bis-Tris gel system (Thermo Fisher Scientific, BN1003BOX) was used according to the manufacturer's instruction using 1% digitonin and NativePAGE 3—12% Bis-Tris gels. Gels were soaked in 0.1% SDS in TBST for 10 min before transfer to 0.45 μm PVDF membranes using a Bio-Rad wet tank blotting system with 0.01% SDS in Tris-glycine transfer buffer containing 10% methanol. The membrane was incubated in 8% acetic acid in TBST for 15 min and subsequently washed with double distilled water. The remaining Coomassie G250 dye was removed with 100% methanol and the membrane used for western blot.

2.6. Subcellular fractionations

Subcellular fractionation was performed as previously described [43]. In brief, cells were homogenized in fractionation buffer (250 mM sucrose, 1 mM EDTA and 10 mM HEPES pH 7.4) containing protease and phosphatase inhibitors using a Potter-Elvehjehm grinder on ice. Homogenates were centrifuged at 500×*g* for 10 min at 4 °C and the supernatant at 100,000×*g* for 30 min at 4 °C to result in membrane pellet. The cytosol fraction in the supernatant was concentrated using 10K Polyethersulfone (PES) membranes (VWR, 516-0229) according to the manufacturer's instructions. The membrane pellet was washed with fractionation buffer. The cytosol and membrane fractions were dissolved with 0.1% SDS and applied to analyses by western blot.

2.7. Immunofluorescent staining and imaging

Cells were cultured on chamber slides (Thermo Fisher Scientific, 154534 PK), fixed with 4% PFA (Sigma Aldrich, P6148) or methanol for 10 min. Tissues were fixed with 4% PFA for 1 h prior to vibratome (Leica) sectioning at 100 μm-thickness. Cells or tissue sections were washed with PBS and 3% BSA and 0.3% Triton-X 100 in PBS were used for blocking and permeabilization for 1 h. Samples were incubated with primary antibodies for 2 h or overnight and Alexa conjugated secondary antibodies (see Table S1) for 1 h. DAPI (Merck Millipore, 508741) diluted in PBS (1 μg/mL) was added to the cells after the secondary antibody for 5 min. Cells and tissue sections were mounted with mounting medium (Dako, S302380-2) and images acquired using a Leica TCS SP5 confocal microscope. Image quantification and co-localization analysis were performed using ImageJ. Colocalization of signals were quantified by JACoP plugin (https://imagej.nih.gov/ij/plugins/track/jacop2.html) in ImageJ. Pearson's correlation coefficient (r) were transformed into z-score by Fisher's *r* to *z* transformation.

2.7.1. EGFP quenching

pBABE-puro mCherry-EGFP-LC3B was obtained from Addgene (#22418, Jayanta Debnath lab) [41]. The plasmid was transiently transfected into adipocytes cultured in live cell imaging chamber slides (ibidi, 80827). Following the amino acid starvation for 1 h, the medium was changed to live cell imaging solution (Thermo Fisher Scientific, A14291DJ) and images were acquired by confocal microscopy maintaining 5% CO_2 and 37 °C during imaging. Relative intensities of mCherry and EGFP were quantified by ImageJ software.

2.7.2. Intracellular pH measurements

pEGFP-LC3 (human) was obtained from Addgene (# 24920, Toren Finkel lab) [49]. The plasmid was transiently transfected into adipocytes. pHrodo Red AM (Thermo Fisher Scientific, P35372) was used to assess intracellular pH following the manufacturer's instruction and imaged as described above. Images were analyzed for co-localization of red and green pixels, and signal intensity by ImageJ software.

2.8. *In vitro* quenching test

The protocol was modified from the published method [43] as described. Adipocytes were loaded with 2.2 mg/mL FITC-Dextran 70,000 (Sigma Aldrich, 46945) in culture medium overnight. The medium was replaced with culture medium or amino acid free DMEM for 1 h. The adipocytes were homogenized in 125 mM KCl, 1 mM EDTA, 50 mM sucrose, 20 mM HEPES pH 7.4, 1% phosphatase and protease inhibitors cocktail using a Potter-Elvehjehm grinder on ice. Big particles were removed by centrifugation at 2,000×*g* for 10 min at 4 °C. The FITC-Dextran loaded vesicles were pelleted by centrifugation at 16,100×*g* for 15 min at 4 °C and the resulting pellet was resuspended in homogenization buffer. Protein concentration was measured using a BCA kit. Particles corresponding to 4—20 μg protein were added with or without 1 μM concanamycin A (Santa Cruz Biotechnology, sc-202111) to flat glass bottom plates to measure FITC fluorescence at 488 nm at 37 °C. Fluorescence intensity was recorded every 2 s for 30 cycles and for additional 120 cycles after addition of 1 mM ATP (Serva Electrophoresis, 10920.01) and 2 mM $MgCl_2$. All intensities were normalized to the baseline of Scr adipocytes samples cultured in regular culture medium. Data transformation was performed according to the Stern-Volmer equation [50] and slopes subsequently calculated.

2.9. Quantitative PCR

Total RNA was extracted from cells and tissues using the RNeasy kit (Qiagen, 74106) following the manufacturer's recommendations. RNA concentrations were measured using a Nano Drop 2000 (Thermo Fisher Scientific) and cDNA was synthesized using 500-1,000 ng RNA and the High-capacity cDNA reverse transcription kit (Thermo Fisher Scientific, 4368813) according to the manufacturer's instruction. SYBR green (Bio-Rad, 172—5125) based real time PCR was performed by using a CFX384 Touch™ Real-Time PCR Detection System (Bio-Rad) with the program 95 °C 30 s, (95 °C 5 s, 60 °C 30 s) × 40 cycles, 95 °C 10 s. The levels of mRNA expression of interest were calculated by delta Ct method to *Tbp* mRNA. Primer sequences: *Pat1* forward (f) CAGCCTGCTGGTGATTGGTA; reverse (r) CCATACATCACCGTGTCCCC, *Pat2* f GTGCCAAGAAGCTGCAGAG; r: TGTTGCCTTTGACCAGATGA, *Pat4* f: TAGTATCACCTGTGCTGGGG; r: GGGCTAGTGTACTGCTGCTC, *Tbp* f: ACCCTTCACCAATGACTCCTATG; r: TGACTGCAGCAAATCGCTTGG, *Pparg*

f: TCCTATTGACCCAGAAAGCGA; r: TGGCATCTCTGTGTCAACCA, *Lc3b* f: AGAGTGGAAGATGTCCGGCT; r: TCTCCCCCTTGTATCGCTCT, *Ucp1* f: CTGCCAGGACAGTACCCAAG; r: TCAGCTGTTCAAAGCACACA.

2.10. Electron microscopy

Preadipocytes were plated on collagen I coated coverslips and differentiated. For electron microscopy, the cells were fixed using 4% paraformaldehyde and 2% glutaraldehyde (Serva Electrophoresis, 23114.01) in PBS followed by staining with 0.5% osmium tetroxide (EMS, 19170). After thorough rinsing in PBS, the sections were dehydrated in graded alcohol and further stained with 1% uranyl acetate (Serva Electrophoresis, 77870) in 70% alcohol. After final dehydration the samples were transferred in propylene oxide (Sigma Aldrich, 82320) and incubated in Durcupan (Sigma Aldrich, 44610-1 EA). After polymerization at 56 °C for 48 h, the cell culture insert was removed and the blocks of resin containing the embedded cells were trimmed and finally cut using an ultra-microtome (Leica Microsystems, Wetzlar, Germany). Ultra-thin sections with an average thickness of 55 nm were transferred on formvar-coated copper grids and stained with lead citrate. Analysis was performed using a Zeiss SIGMA electron microscope (Zeiss NTS, Oberkochen, Germany) equipped with a STEM detector and ATLAS software.

2.11. Cellular respirometry

Oxygen consumption of brown adipocytes was measured by an XF96 Extracellular Flux Analyzer (Seahorse Bioscience) as described in [40]. Cellular respirometry was performed at day 7–8 days of differentiation. Cells were incubated in amino acid-free medium with 10% dialyzed FBS for 1 or 24 h before the analyses. Unstarved and recovery conditions were run in XF DMEM (Agilent Technologies, 103575-100) with 25 mM glucose, 2 mM GlutaMAX (Gibco, 35050038), and 0.2% fatty acid-free BSA, while amino acid-starved conditions were run in amino acid-free medium with 0.2% fatty acid-free BSA, following incubation for 30 min. After measurement of basal respiration, compounds were sequentially injected as follows: 5 μM oligomycin, 1 μM isoproterenol, 7.5 μM FCCP, and 5 μM Ant A with 3 μM rotenone. Basal and maximal respiration are mean values of the 4 cycles before oligomycin injection and 3 cycles after FCCP injection, respectively. ATP-coupled respiration was calculated by subtraction of the value at the third measurement after oligomycin injection from the basal respiration. Proton-leak was calculated by subtraction of the mean of values after Ant A and rotenone from the value at the third measurement after oligomycin injection. Isoproterenol-response was calculated by subtraction of the value at the third measurement after oligomycin injection from the maximal value after isoproterenol injection.

2.12. Statistical analysis

GraphPad PRISM 6 and 8 were used for statistical analysis. Error bars, P values, sample size and statistical tests are detailed in the respective figure legends.

2.13. Data availability

All data and materials are available upon request from the corresponding author.

3. RESULTS AND DISCUSSION

3.1. Brown adipose tissue is sensitive to energy deprivation by fasting

To study the fasting response of metabolically important tissues, 8 weeks old chow diet (CD)-fed male wild-type C57BL/6 mice were fasted overnight. Overnight starvation significantly reduced blood glucose levels but did not significantly reduce body weight or weights of individual tissues in these lean CD-fed animals (Figure 1A).

Overnight fasting did not change the mRNA expression of the autophagy marker LC3b in BAT, or any other tissue investigated, despite a tendency for increased expression in subcutaneous and perigonadal white fat (SCF and PGF, respectively) (Figure 1B). In contrast, expression of the brown/beige adipocyte specific genes uncoupling protein-1 (UCP-1) and the amino acid transporter PAT2 was significantly reduced (Figure 1B). However, UCP-1 protein levels were not reduced following an overnight fast (Figure 1C). PAT2 protein levels could not be determined due to the unavailability of specific antibodies for murine PAT2. Albeit we did not observe differences in the gene expression of LC3b upon fasting, a strong conversion from the cytosolic LC3 type I to the autophagosome incorporated LC3 type II was observed in skeletal muscle (tibialis anterior: TA) and BAT (Figure 1C). Fasting upregulated LC3 levels in the liver, but did not result in increased conversion from LC type I to type II. These changes were not observed in SCF and PGF (Figure 1C). The increase in LC3 type II in BAT but not white adipose tissues was also confirmed by immunofluorescence stainings of LC3 (Figure 1D). Thus, BAT unlike WAT induces autophagy in response to an overnight fast similarly to skeletal muscle indicating a high sensitivity of BAT towards fluctuations in nutrient availabilities.

3.2. PAT2 localizes to the lysosome in brown preadipocytes

We previously identified PAT2 as highly expressed in brown and beige adipocytes [29] and the co-regulation with UCP-1 in response to an overnight fast prompted us to investigate its potential role in orchestrating the amino acid related fasting response. To study the function of PAT2 in brown preadipocytes and adipocytes, we established brown preadipocyte cell lines stably overexpressing HA-tagged PAT2 (PAT2-HA) or depleted of PAT2 (shPAT2) (Figure 2A and Fig. S1A). Using this overexpression system also allowed us visualizing the distribution of PAT2 due to the lack of a PAT2 antibody detecting the endogenous levels.

As previously reported [29], PAT2 mRNA expression is very low in preadipocytes and strongly induced upon brown adipocyte differentiation (Figure 2A). Interestingly, protein levels of stably overexpressed PAT2 were also much lower in brown preadipocytes compared to fully differentiated mature brown adipocytes (Fig. S1A). PAT2-HA expression is under the control of the same promoter in both cell types. Thus, we suspected that brown adipocytes had a reduced degradation of PAT2 protein compared to preadipocytes. Lysosomal protein degradation is the default pathway for turnover of cell surface proteins and plays an important role in regulating mTORC1 activation and autophagy [36–39]. Indeed, overexpressed PAT2 predominantly localized to lysosomes in preadipocytes (Fig. S1B). Treatment of brown preadipocytes with the vATPase inhibitor bafilomycin A1 tended to increase PAT2-HA protein levels in preadipocytes (Fig. S1C) suggesting a continuous turnover via lysosomal degradation of PAT2 in preadipocytes.

3.3. PAT2 translocates from the plasma membrane to the lysosome upon amino acid depletion

In contrast to preadipocytes, exogenously overexpressed PAT2 predominantly localized to the plasma membrane in mature brown adipocytes (Figure 2B), consistent with our previous findings on the endogenous protein [29]. Knockdown or overexpression of PAT2 did not impair lipid accumulation (Figs. S2A and S2B) and expression of the key adipogenic transcription factor PPARγ (Figure 2C,D, Fig. S2C),

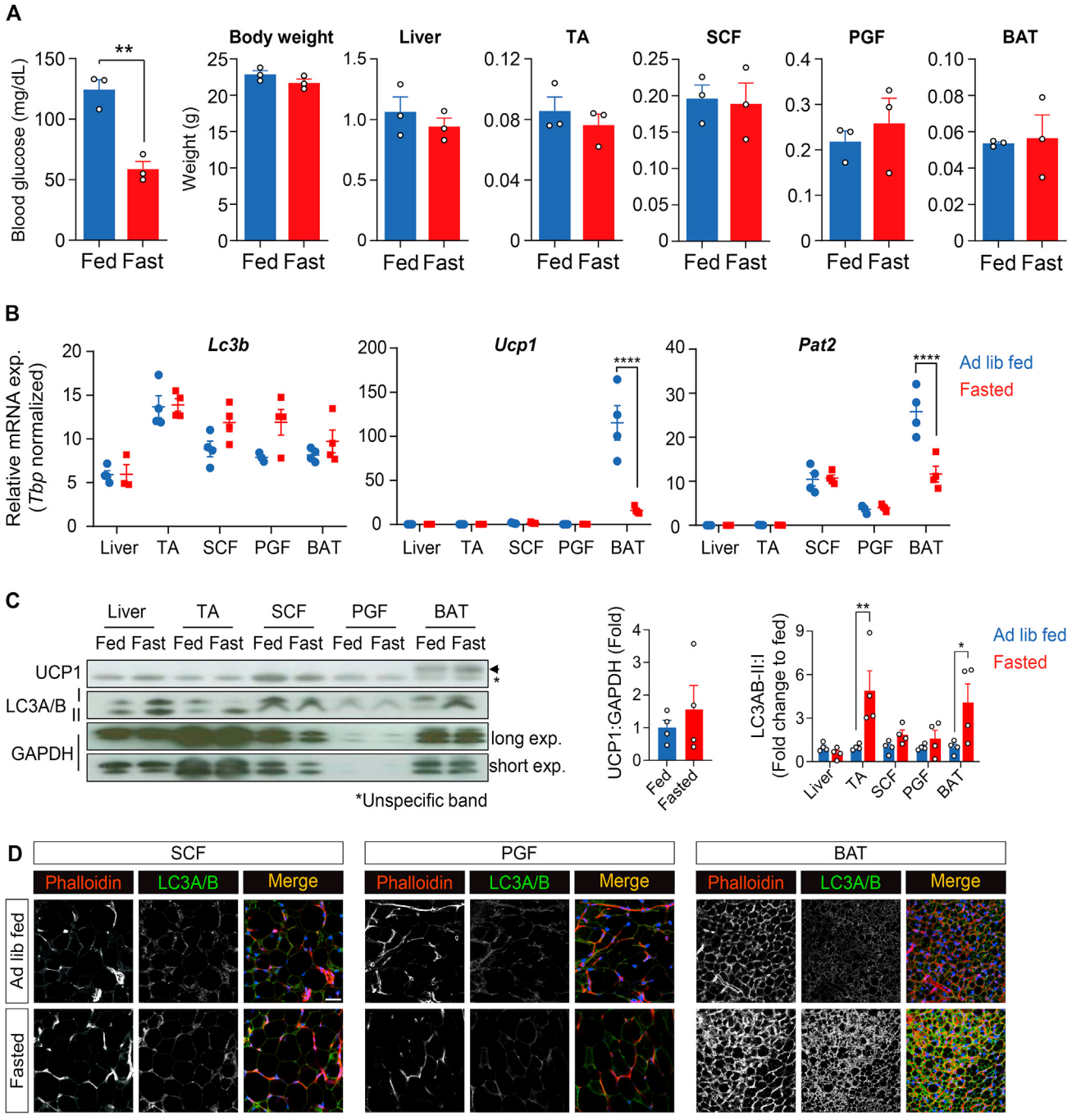

Figure 1: BAT induces autophagy upon overnight fasting. (**A**) Blood glucose, body weight, and weights of liver, tibialis anterior (TA), subcutaneous fat (SCF), perigonadal fat (PGF) and brown adipose tissue (BAT) from ad libitum fed and overnight fasted mice (n = 3). $^{**}p < 0.01$; unpaired *t*-test; Error bars show SEM. (**B**) Quantitative PCR of LC3B, UCP-1 and PAT2 mRNA expression in liver, TA, SCF, PGF and BAT from ad libitum fed and overnight fasted mice. n = 4; $^{****}p < 0.0001$; RM two-way ANOVA with Tukey's post hoc test. (**C**) Western blots from ad libitum fed and overnight fasted mice. Arrow indicates specific and asterisk indicates unspecific signals. Relative protein expression of UCP1 normalized by GAPDH expression is shown as fold change in the middle panel. Relative protein expression of LC3AB-II to LC3AB-I are shown as fold change to ad lib fed mice for respective tissue (right panel). n = 4 biological replicates. Error bars show SEM. $^{**}p < 0.01$, $^{*}p < 0.05$; two-way ANOVA with Sidak's multiple comparisons test. (**D**) Representative immunofluorescence stainings of LC3AB and DAPI for adipose tissues from ad libitum fed and overnight fasted mice. Scale bar shows 40 μm.

despite increased mRNA levels of PPARγ at day 8 in PAT2-HA brown adipocytes. In contrast, mRNA and protein levels of the brown adipocyte specific protein UCP-1 were elevated in both PAT2-HA and shPAT2 adipocytes compared to control cells (Figure 2C,D, Fig. S2C). However, assessment of oxygen consumption rates in shPAT2 and PAT2-HA brown adipocytes did not reveal major differences between the cell lines. In contrast to our expectation we even observed a reduction in isoproterenol induced and FCCP induced maximal respiration of both shPAT2 and PAT2-HA brown adipocytes (Figure 2E and S3A-E). These data could suggest a dissociation between UCP-1

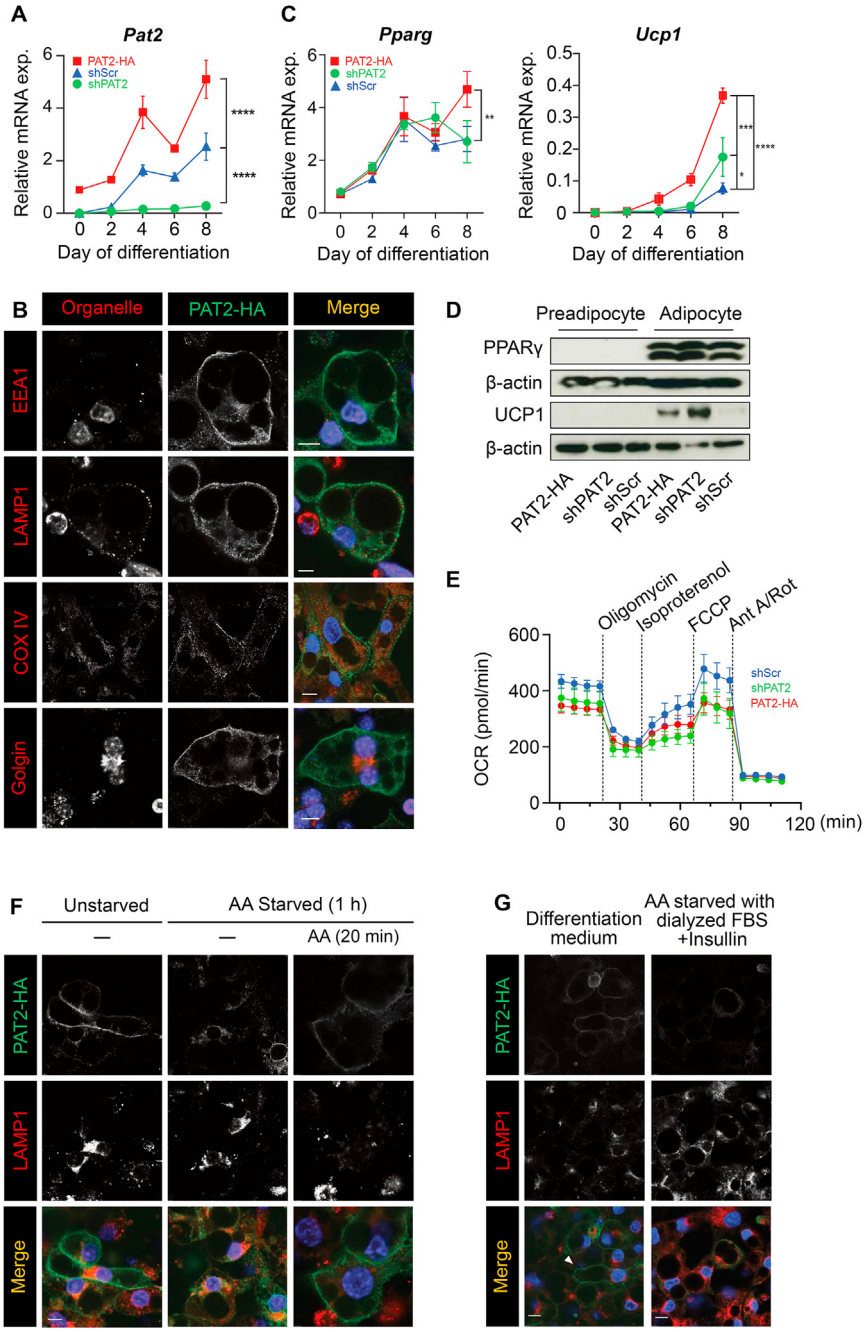

Figure 2: Subcellular localization of PAT2 in brown adipocytes depends on extracellular amino acid availability. (**A**) PAT2 mRNA levels at indicated time points during differentiation ($n = 3–6$ biological replicates for Quantitative PCR). ****$p < 0.0001$, RM two-way ANOVA with Tukey's post hoc test. (**B**) Immunofluorescence staining of PAT2-HA and different organelle markers (EEA1 for late endosome; LAMP1 for lysosome; COX IV for mitochondria; Golgin for golgi apparatus) in brown adipocytes (day 8). Scale bar shows 7.5 μm. (**C**) PPARγ and UCP-1 mRNA levels at indicated time points during differentiation ($n = 3–6$ biological replicates for Quantitative PCR).*$p < 0.05$; **$p < 0.01$; ***$p < 0.001$; ****$p < 0.0001$, RM two-way ANOVA with Tukey's post hoc test. (**D**) PPARγ and UCP-1 protein levels in preadipocytes at day 0 and adipocytes at day 8 of differentiation. Representative images of three (PPARγ) and four (UCP1) independent experiments. (**E**) Cellular oxygen consumption rate (OCR) in shScr, shPAT2, and PAT2-HA brown adipocytes. Data are mean of four biological replicates. Error bars show SEM.(**F**) Immunofluorescence staining of PAT2-HA and LAMP1 in PAT2-HA brown adipocytes under normal culture conditions or serum and amino acid starvation for 1 h with or without re-stimulation with amino acids for 20 min. Scale bars show 7.5 μm. (**G**) Immunofluorescence staining of PAT2-HA and LAMP1 in PAT2-HA brown adipocytes under normal culture condition or serum and amino acid starvation with 100 nM insulin for 1 h. Arrowhead indicates plasma membrane staining. Scale bars show 10 μm.

content, its activity and mitochondrial mass in brown adipocytes with either deficiency or overexpression of PAT2. The phenotype of PAT2 overexpression and knockdown is similar to the phenotype observed upon modulation of PAT1 levels [39,46] and could indicate a role of PAT2 in lysosomal amino acid turnover and mTORC1 activation. This and the difference in localization of PAT2 between preadipocytes and adipocytes prompted us to test the response of PAT2 to serum and amino acid starvation. Serum and amino acid depletion for 1 h induced

a translocation of PAT2 from the plasma membrane to the lysosome, which was rapidly reverted by replenishing amino acids (Figure 2F). The selectivity of the observed translocation to amino acid depletion was confirmed by inducing translocation using amino acid withdrawal in the presence of 10% dialyzed FBS (Figure 2G). Thus, PAT2 resides at the cell surface when ample extracellular amino acid levels are available but rapidly internalizes and translocates to the lysosome upon amino acid withdrawal. This raised the possibility that PAT2 contributes to the lysosomal amino acid turnover upon amino acid starvation.

3.4. PAT2 facilitates the recruitment of the V1 domain to assemble the vATPase upon amino acid starvation

Assessment of intracellular pH, using a membrane permeable pH sensitive dye in brown adipocytes, transiently transfected with EGFP-LC3 to visualize autolysosomes, revealed decreased lysosomal pH in control cells following amino acid starvation, whereas this was strongly blunted in shPAT2 cells (Figure 3A and Fig. S4A). PAT2-HA adipocytes showed decreased lysosomal pH already in regular culture conditions (Figure 3A and Fig. S4A). To independently verify this observation we quantified proton dependent EGFP quenching in the autolysosome using a transiently transfected mCherry-EGFP-LC3 construct [41]. This showed reduced quenching of EGFP in shPAT2 and PAT2-HA adipocytes upon amino acid starvation for 1 h, when expressed as EGFP:mCherry ratio (Figure 3B).

Thus, loss of PAT2 increased lysosomal pH, whereas overexpression of PAT2-HA resulted in hyperacidification of the lysosome. Albeit, PAT2 in itself is able to transport protons, lysosomal acidification is thought to be predominantly driven by the vATPase [42]. Indeed, vATPase inhibition using bafilomycin A1 confirmed the dependency of starvation induced lysosomal acidification on vATPase activity in our cell lines (Fig. S4B). Hence, PAT2 regulates lysosomal pH via modulation of vATPase activity.

Measurements of vATPase activity through pH dependent quenching of FITC-dextran [43] showed enhanced proton pumping in response to amino acid starvation in lysosomal enriched fractions of PAT2-HA cells. This was blunted in shPAT2 cells (Figure 3C). To check the dependency on lysosomal PAT2 amino acid transport activity upon amino acid starvation, quenching experiments were performed with two PAT2 inhibitors, αMTP or 5HTP [44] in lysosomal fractions isolated from control brown adipocytes (Figure 3D). Only higher concentration of αMTP suppressed quenching of FITC (Figure 3D), but a similar inhibition was observed in PAT2 knockdown brown adipocytes, suggesting an off-target effect of the inhibitor at this concentration. However, both PAT2 inhibitors at 5 mM retained PAT2 at the cell surface upon amino acid starvation. Thus the amino acid transport activity is dispensable for the function of PAT2 in regulating vATPase activity but important for its cell surface localization (Fig. S4C).

Regulation of vATPase assembly is the main mechanism regulating vATPase activity [45]. Western blots did not indicate differences in protein levels of V1B2 between shScr, shPAT2 and PAT2-HA adipocytes (Fig. S4D). Using blue native PAGEs we detected the fully assembled vATPase at >720 kDa, as determined by an overlapping signal of V1B2 and V0D1 (Figure 3E). Both control and PAT2-HA cells increased the amount of fully assembled vATPase upon amino acid starvation, whereas shPAT2 cells had strongly decreased amounts of vATPase both at baseline and upon amino acid starvation. Thus, the observed increase in lysosomal pH in shPAT2 adipocytes appears as the consequence of impaired assembly of the full size vATPase, while the decreased pH upon overexpression of PAT2 could be attributed to a slightly increased vATPase assembly and proton pumping activity. Membrane and cytosolic fractionations independently confirmed reduced vATPase assembly upon amino acid depletion in shPAT2 adipocytes (Fig. S4E). Using co-immunoprecipitations we showed that PAT2-HA interacts with the V1B2 subunit of the vATPase V1 domain, but not V0D1, a V0 subunit, in amino acid starved adipocytes (Figure 3F). However, unlike PAT1 [39], we were unable to identify an interaction of PAT2 with either mTOR or RagC (Figure 3F). This suggests a mechanism whereby PAT2, upon translocation from the plasma membrane via the endosome to the lysosome, facilitates the assembly of the vATPase by recruiting the V1 domain to the lysosomal surface, where it interacts with the V0 subunit. Because of loss of PAT2, vATPase assembly is perturbed resulting in an overall decrease in lysosomal acidification. Conversely, overexpression of PAT2 increases vATPase assembly, activity and lysosomal acidification.

3.5. PAT2 regulates autophagosome size and mTORC1 activation upon starvation

We then tested if the altered lysosomal acidification impairs autolysosome formation and function. Electron microscopy did not reveal differences in autophagosome numbers between the three cell lines (Figure 3G,H). Thus, overexpression or depletion of PAT2 did not impair autophagosome formation per se. In line with this, we also did not observe differences in LC3 mRNA expression upon overexpression or depletion of PAT2 (Fig. S4F). However, differences in mean autophagosome size were observed upon starvation (Figure 3I). Thus, we tested if PAT2 regulates autophagosome and lysosome fusion. Co-immunostainings of LAMP1 and LC3 revealed reduced co-localization of these lysosome and autophagosome markers, respectively, in both shPAT2 and PAT2-HA cells (Figure 3J,K). Thus, both too high and too low lysosomal pH appear to inhibit autophagosome and lysosome fusion. To further investigate the impaired autolysosome function we studied mTORC1 re-activation upon prolonged amino acid depletion. Amino acid deprivation resulted in rapid dephosphorylation followed by rephosphorylation of the main mTORC1 effector protein S6K in control adipocytes (Figure 3L and M and Fig. S4G). However, in line with impaired lysosomal pH and autolysosome formation, prolonged starvation resulted in impaired re-phosphorylation of S6K in both shPAT2 and PAT2-HA brown adipocytes (Figure 3L,M). Phosphorylation of mTOR was not changed (Fig. S4G), suggesting that loss or gain of PAT2 alters autolysosomal amino acid release rather than growth factor signaling. Surprisingly, both knockdown and overexpression of PAT2, albeit showing opposing effects on vATPase assembly and lysosomal acidification, resulted in similar phenotypes with regards to autolysosome formation and mTORC1 re-activation. A similarly decreased S6K phosphorylation was also observed upon both knockdown [46] and overexpression [39] of PAT1, possibly due to impairments of amino-acid dependent re-location of mTOR to the lysosome [47] and prevention of amino acid accumulation in the lysosomal lumen activating mTORC1 [39], respectively. In contrast to PAT2, PAT1 and SNAT family members constitutively localize to the lysosomal membrane where they interact with the mTORC1 supercomplex requiring vATPase [39]. However, the role of PAT2 appears more indirect as PAT2-HA could not be co-precipitated with either mTOR or RagC in control or amino acid starved conditions in brown adipocytes (Figure 3F). This suggests that PAT2 regulates mTORC1 activity via its function on vATPase assembly, lysosomal acidification and thereby lysosomal amino acid release.

To understand the bioenergetic consequences of loss and gain of PAT2 in brown adipocytes we assessed oxygen consumption and uncoupled respiration in shScr, shPAT2 and PAT2-HA brown adipocytes (Figure 3N and S3A-E). One-hour amino acid deprivation did not induce significant changes between the cell lines. Twenty-four-hour amino

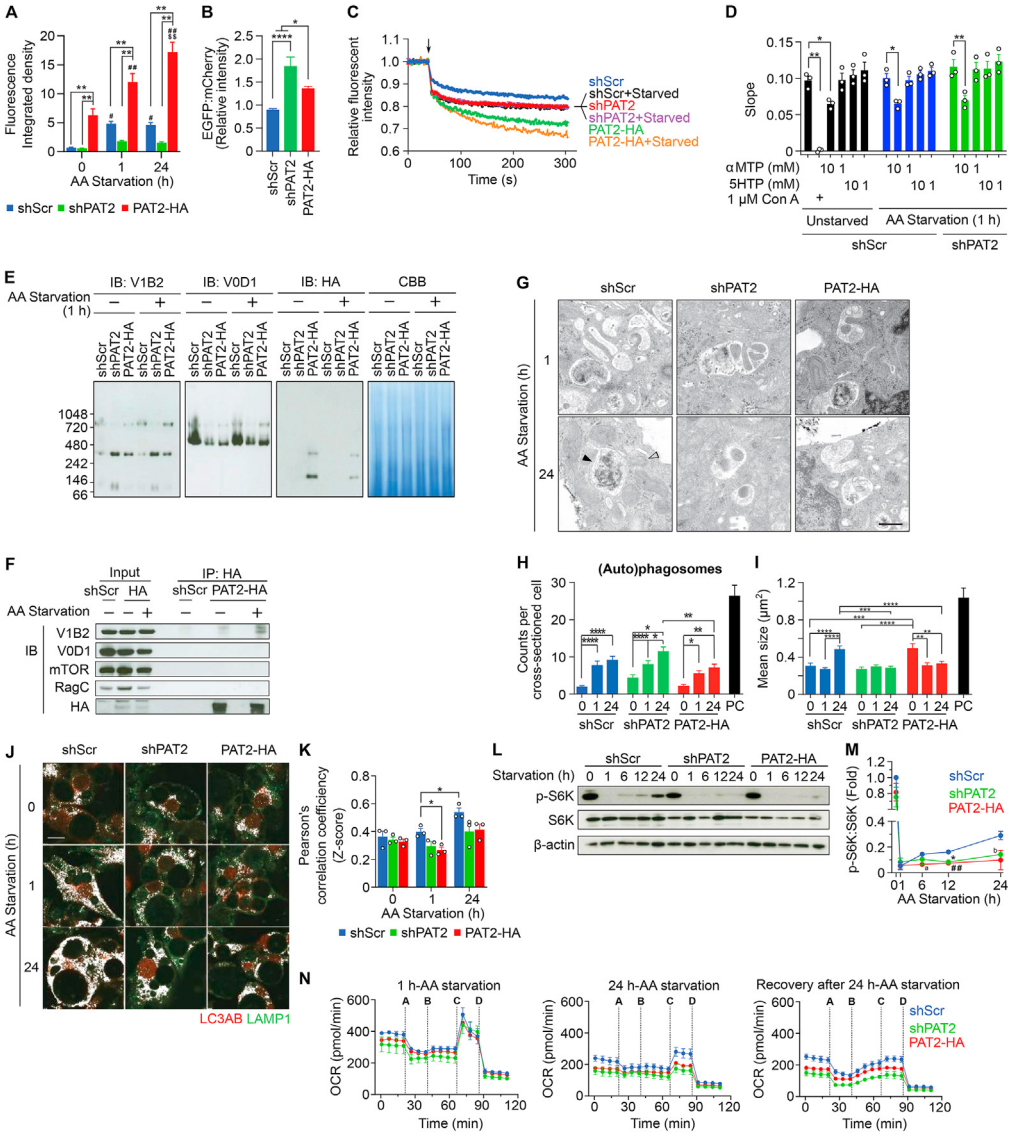

Figure 3: PAT2 regulates assembly and proton pumping efficiency of the lysosomal vATPase. (**A**) Fluorescence integrated density of the signal with intracellular pH indicator in shScr, shPAT2 and PAT2-HA adipocytes in control medium or amino acid and serum free medium for one or 24 h, shown in Figure 3A. Thirty intracellular vesicles where the LC3-EGFP and intracellular pH indicator colocalized across three different areas of each cell line at each time-point were chosen. RM two-way ANOVA with Tukey's post hoc test; **, ## and $^{\$\$}p < 0.01$, * and $^{\#}p < 0.05$, error bars show SEM. The symbol # and $ indicate comparisons with unstarved condition or one hour-starvation condition, respectively within each cell line. (**B**) Quantification of EGFP quenching, in cells transiently transfected with mCherry-EGFP-LC3, upon one hour-amino acid starvation (n = 28–33 cells per condition, ****$p < 0.0001$, *$p < 0.05$, one-way ANOVA, Tukeys' post hoc test; error bars show SEM). (**C**) Lysosomal and endosomal FITC-dextran quenching in shScr, shPAT2 and PAT2-HA brown adipocytes in control and amino acid free DMEM for 1 h. Arrow indicates timing of injection of compounds triggering quenching. (**D**) Lysosomal acidification rates in shScr and shPAT2 brown adipocytes under normal or one hour-amino acid starvation condition, followed by acute treatment of PAT2 inhibitors αMTP or 5HTP to isolated lysosomal suspension. Acute treatment with 1 μM Concanamycin A (Con A) was used as negative control. Lysosomal acidification rates shown as slopes were calculated from liner regression curves between reciprocal values of fluorescent intensity. n = 3 biological replicates. Error bars show SEM. One-way ANOVA with Sidak's multiple comparisons test. *$p < 0.05$, **$p < 0.01$. (**E**) BN-PAGE for vATPase assembly of whole cell lysates from shScr, shPAT2 and PAT2-HA brown adipocytes in control or amino acid free DMEM (1 h). (**F**) Co-immunoprecipitation of PAT2-HA with components of the lysosomal vATPase (V1B2 and V0D1), mTOR and RagC in differentiated brown adipocytes. (**G**) Representative electron microscopy images for shScr, shPAT2 and PAT2-HA cells upon amino acid starvation for one and 24 h. Black arrowhead indicates autophagosomes, open arrowhead indicates lysosome. Scale bar shows 500 nm. (**H**) Quantification of autophagosome number (n = 30 cross-sectioned cells) and (**I**) mean autophagosome size (n = 74–161 autophagosomes in cross-sectioned cells) in shScr, shPAT2 and PAT2-HA adipocytes in regular culture conditions and upon one or 24 h-amino acid starvation shown in panel G. Positive control (PC) was excluded from statistic; RM two-way ANOVA with Tukey's post hoc test; ****$p < 0.0001$, ***$p < 0.001$, **$p < 0.01$, *$p < 0.05$, error bars show SEM. (**J**) Immunostaining of LAMP1 and LC3AB in shScr, shPAT2 and PAT2-HA adipocytes upon 0, 1 or 24 h-amino acid starvation. Colocalized pixels are shown in white. Scale bar shows 10 μm. (**K**) Colocalization of signals with LC3AB and LAMP1 shown in panel J analyzed by Pearson's correlation coefficient (r). The data are shown with z-score computed by Fisher's r to z transformation. n = 3 biological replicates RM two-way ANOVA with Tukey's post hoc test; *$p < 0.05$, error bars show SEM. (**L**) Western blot for S6K phosphorylation in shScr, shPAT2 and PAT2-HA brown adipocytes upon amino acid and serum depletion for 1, 6, 12 or 24 h. (**M**) Quantification of relative S6K phosphorylation is normalized to respective total S6K level. (n = 3 biological replicates; RM two-way ANOVA with Tukey's post hoc test; $^{a}p = 0.0729$: shScr vs. PAT2-HA at 6 h-starvation; *$p < 0.05$: shScr vs. shPAT2 at 12 h-starvation; $^{\#\#}p < 0.01$: shScr vs. PAT2-HA at 12 h-starvation; $^{b}p = 0.0902$: shScr vs. shPAT2 at 24 h-starvation; error bars show SEM). (N) Cellular oxygen consumption rates (OCR) in shScr, shPAT2, and PAT2-HA brown adipocytes upon amino acid (AA)-starvation for 1 h or 24 h (three biological replicates), or amino acid replenishment after 24 h-AA starvation (n = 4). Compounds were injected as follows; A: oligomycin, B: isoproterenol, C: FCCP, and D: Ant A/rotenone. Error bars show SEM.

acid starvation, which is associated with impaired mTORC1 activity in shPAT2 and PAT2-HA adipocytes, led to a defective respiration in shPAT2 adipocytes, with a similar trend in PAT-HA adipocytes (Figure 3N). Starvation did not alter expression of either PAT2 or PAT2 in either cell line compared to the unstarved condition. Expression of PAT1 was increased in shPAT2 cells in the unstarved condition compared to control and PAT2-HA cells, but its expression was not different among the three cell lines upon 24 h amino acid starvation (Fig. S4H). When adipocytes were measured in amino acid-containing medium following a 24 h-amino acid deprivation, both shPAT2 and PAT2-HA cells showed reduced oxygen consumption compared to control cells. The effect of either knockdown or overexpression of PAT2 on lysosomal acidification and vATPase assembly were opposed, whereas the impact on autophagolysosome formation and mTORC1 activation was similar. Thus it is very likely that the observed impact on mitochondrial activity is a consequence of either impaired starvation induced mTORC1 activity or autophagy. The latter could suggest a role of PAT2 in regulating mitochondrial turnover via regulating mitophagy.

4. CONCLUSIONS AND LIMITATIONS

In summary, we identified the amino acid transporter PAT2 to promote lysosomal acidification upon reductions in extracellular amino acid availability in brown adipocytes. In response to amino acid depletion, PAT2 translocates from the plasma membrane to the lysosome, where it facilitates the assembly of the vATPase promoting lysosomal acidification, which is essential for the induction of autophagy. However, our study also revealed that PAT2 protein levels need to be tightly regulated as both too little (as seen in the knockdown) or too much (as seen in the overexpression), impair autophagosome and lysosome fusion. Thus, the expression of PAT2 in brown adipose tissue and the here described functions suggest that BAT has a very high sensitivity towards changes in extracellular amino acid levels to induce autophagy. It will be very important to investigate the consequences of loss or gain of function of PAT2 on mitophagy, mitochondrial turnover and the overall thermogenic capacity of brown adipocytes in the future.
However, the current study also has technical limitations that need to be considered when assessing the role of PAT2 *in vivo*, especially in humans. We were unable to study the endogenous protein levels and dynamics due to a lack of a mouse specific PAT2 antibody. Thus, we will continue our efforts to create a murine PAT2 specific antibody to confirm the endogenous protein translocation. Moreover, we performed all experiments in an immortalized brown adipocyte cell line and stable knockdown or overexpression of PAT2. Thus, future studies using PAT2 knockout or PAT2 overexpressing mice will be important to also assess the physiological role of PAT2 in BAT *in vivo*.

AUTHOR CONTRIBUTIONS

JW, YO and SU designed and conducted experiments and wrote the manuscript. RK and IS conducted experiments. MK conducted the electron microcopy experiments. YL and JO performed cellular respirometry. RF and SMH contributed to study design and data analysis.

ACKNOWLEDGEMENTS

This work was supported funds from the German Research Foundation as well as from the project Aging and Metabolic Programming (AMPro). JW was supported by the China Scholarship Council. YO received support through the Post-doctoral Fellowship program from The Uehara Memorial Foundation, Japan (201830047) and the Alexander von Humboldt-Stiftung, Germany. We would like to express our appreciation to Prof. Dr. Tsuneo Imanaka (Hiroshima International University, Japan), Dr. Kosuke Kawaguchi (University of Toyama, Japan), Dr. Takumi Okamoto (Nagasaki University, Japan) and Dr. Yuichi Watanabe (Showa University, Japan) for giving advice about lysosomal fractionation and co-immunoprecipitation.

CONFLICT OF INTEREST

None declared.

APPENDIX A. SUPPLEMENTARY DATA

Supplementary data to this article can be found online at https://doi.org/10.1016/j.molmet.2022.101508.

REFERENCES

[1] Klepac, K., Georgiadi, A., Tschop, M., Herzig, S., 2019. The role of brown and beige adipose tissue in glycaemic control. Molecular Aspects of Medicine 68: 90–100.
[2] Nedergaard, J., Cannon, B., 2018. Brown adipose tissue as a heat-producing thermoeffector. Handbook of Clinical Neurology 156:137–152.
[3] Townsend, K.L., Tseng, Y.H., 2014. Brown fat fuel utilization and thermogenesis. Trends in Endocrinology and Metabolism 25(4):168–177.
[4] Hoeke, G., Kooijman, S., Boon, M.R., Rensen, P.C., Berbee, J.F., 2016. Role of Brown fat in lipoprotein metabolism and atherosclerosis. Circulation Research 118(1):173–182.
[5] Heeren, J., Scheja, L., 2018. Brown adipose tissue and lipid metabolism. Current Opinion in Lipidology 29(3):180–185.
[6] Hankir, M.K., Klingenspor, M., 2018. Brown adipocyte glucose metabolism: a heated subject. EMBO Reports 19(9).
[7] Li, Y., Schnabl, K., Gabler, S.M., Willershauser, M., Reber, J., Karlas, A., et al., 2018. Secretin-activated Brown fat mediates prandial thermogenesis to induce satiation. Cell 175(6):1561–1574 e1512.
[8] Mills, E.L., Pierce, K.A., Jedrychowski, M.P., Garrity, R., Winther, S., Vidoni, S., et al., 2018. Accumulation of succinate controls activation of adipose tissue thermogenesis. Nature 560(7716):102–106.
[9] Okla, M., Kim, J., Koehler, K., Chung, S., 2017. Dietary factors promoting Brown and beige fat development and thermogenesis. Advances in Nutrition 8(3):473–483.
[10] Ramirez, A.K., Lynes, M.D., Shamsi, F., Xue, R., Tseng, Y.H., Kahn, C.R., et al., 2017. Integrating extracellular Flux measurements and genome-scale modeling reveals differences between Brown and white adipocytes. Cell Reports 21(11):3040–3048.
[11] Oelkrug, R., Polymeropoulos, E.T., Jastroch, M., 2015. Brown adipose tissue: physiological function and evolutionary significance. Journal of Comparative Physiology B 185(6):587–606.
[12] Ruiz-Ojeda, F.J., Wang, J., Backer, T., Krueger, M., Zamani, S., Rosowski, S., et al., 2021. Active integrins regulate white adipose tissue insulin sensitivity and brown fat thermogenesis. Molecular Metabolism 45:101147.
[13] Hankir, M.K., Cowley, M.A., Fenske, W.K., 2016. A BAT-centric approach to the treatment of diabetes: turn on the brain. Cell Metabolism 24(1):31–40.
[14] Kuruvilla, R., 2019. Why brown fat has a lot of nerve. Nature 569(7755):196–197.
[15] Lopez-Soriano, F.J., Alemany, M., 1989. Effect of alanine on in vitro glucose utilization by rat interscapular brown adipose tissue. Biochimica et Biophysica Acta 1010(3):338–341.
[16] Wanders, D., Stone, K.P., Dille, K., Simon, J., Pierse, A., Gettys, T.W., 2015. Metabolic responses to dietary leucine restriction involve remodeling of

adipose tissue and enhanced hepatic insulin signaling. BioFactors 41(6): 391–402.
[17] Wu, Z., Satterfield, M.C., Bazer, F.W., Wu, G., 2012. Regulation of brown adipose tissue development and white fat reduction by L-arginine. Current Opinion in Clinical Nutrition and Metabolic Care 15(6):529–538.
[18] Condon, K.J., Sabatini, D.M., 2019. Nutrient regulation of mTORC1 at a glance. Journal of Cell Science 132(21).
[19] Zhang, X., Wu, D., Wang, C., Luo, Y., Ding, X., Yang, X., et al., 2019. Sustained activation of autophagy suppresses adipocyte maturation via a lipolysis-dependent mechanism. Autophagy, 1–15.
[20] Ferhat, M., Funai, K., Boudina, S., 2018. Autophagy in adipose tissue physiology and pathophysiology. Antioxid Redox Signal.
[21] Cairo, M., Villarroya, J., 2020. The role of autophagy in brown and beige adipose tissue plasticity. Journal of Physiology & Biochemistry 76(2):213–226.
[22] Dikic, I., Elazar, Z., 2018. Mechanism and medical implications of mammalian autophagy. Nature Reviews Molecular Cell Biology 19(6):349–364.
[23] Galluzzi, L., Pietrocola, F., Levine, B., Kroemer, G., 2014. Metabolic control of autophagy. Cell 159(6):1263–1276.
[24] Mizushima, N., 2018. A brief history of autophagy from cell biology to physiology and disease. Nature Cell Biology 20(5):521–527.
[25] Shen, Y., Su, Y., Silva, F.J., Weller, A.H., Sostre-Colon, J., Titchenell, P.M., et al., 2020. Shared PPARalpha/gamma target genes regulate Brown adipocyte thermogenic function. Cell Reports 30(9):3079–3091 e3075.
[26] Huber, K., Hofer, D.C., Trefely, S., Pelzmann, H.J., Madreiter-Sokolowski, C., Duta-Mare, M., et al., 2019. N-acetylaspartate pathway is nutrient responsive and coordinates lipid and energy metabolism in brown adipocytes. Biochimica et Biophysica Acta (BBA) - Molecular Cell Research 1866(3):337–348.
[27] Kissing, S., Hermsen, C., Repnik, U., Nesset, C.K., von Bargen, K., Griffiths, G., et al., 2015. Vacuolar ATPase in phagosome-lysosome fusion. Journal of Biological Chemistry 290(22):14166–14180.
[28] McGuire, C., Cotter, K., Stransky, L., Forgac, M., 2016. Regulation of V-ATPase assembly and function of V-ATPases in tumor cell invasiveness. Biochimica et Biophysica Acta 1857(8):1213–1218.
[29] Ussar, S., Lee, K.Y., Dankel, S.N., Boucher, J., Haering, M.F., Kleinridders, A., et al., 2014. ASC-1, PAT2, and P2RX5 are cell surface markers for white, beige, and brown adipocytes. Science Translational Medicine 6(247): 247ra103.
[30] Schioth, H.B., Roshanbin, S., Hagglund, M.G., Fredriksson, R., 2013. Evolutionary origin of amino acid transporter families SLC32, SLC36 and SLC38 and physiological, pathological and therapeutic aspects. Molecular Aspects of Medicine 34(2–3):571–585.
[31] Thwaites, D.T., Anderson, C.M., 2011. The SLC36 family of proton-coupled amino acid transporters and their potential role in drug transport. British Journal of Pharmacology 164(7):1802–1816.
[32] Rubio-Aliaga, I., Boll, M., Vogt Weisenhorn, D.M., Foltz, M., Kottra, G., Daniel, H., 2004. The proton/amino acid cotransporter PAT2 is expressed in neurons with a different subcellular localization than its paralog PAT1. Journal of Biological Chemistry 279(4):2754–2760.
[33] Boll, M., Foltz, M., Rubio-Aliaga, I., Kottra, G., Daniel, H., 2002. Functional characterization of two novel mammalian electrogenic proton-dependent amino acid cotransporters. Journal of Biological Chemistry 277(25):22966–22973.
[34] Kennedy, D.J., Gatfield, K.M., Winpenny, J.P., Ganapathy, V., Thwaites, D.T., 2005. Substrate specificity and functional characterisation of the H+/amino acid transporter rat PAT2 (Slc36a2). British Journal of Pharmacology 144(1):28–41.
[35] Foltz, M., Oechsler, C., Boll, M., Kottra, G., Daniel, H., 2004. Substrate specificity and transport mode of the proton-dependent amino acid transporter mPAT2. European Journal of Biochemistry 271(16):3340–3347.
[36] Abu-Remaileh, M., Wyant, G.A., Kim, C., Laqtom, N.N., Abbasi, M., Chan, S.H., et al., 2017. Lysosomal metabolomics reveals V-ATPase- and mTOR-dependent regulation of amino acid efflux from lysosomes. Science 358(6364):807–813.
[37] Perera, R.M., Zoncu, R., 2016. The lysosome as a regulatory hub. Annual Review of Cell and Developmental Biology 32:223–253.
[38] Wu, X., Zhao, L., Chen, Z., Ji, X., Qiao, X., Jin, Y., et al., 2016. FLCN maintains the leucine level in lysosome to stimulate mTORC1. PLoS One 11(6): e0157100.
[39] Zoncu, R., Bar-Peled, L., Efeyan, A., Wang, S., Sancak, Y., Sabatini, D.M., 2011. mTORC1 senses lysosomal amino acids through an inside-out mechanism that requires the vacuolar H(+)-ATPase. Science 334(6056):678–683.
[40] Li, Y., Fromme, T., Schweizer, S., Schottl, T., Klingenspor, M., 2014. Taking control over intracellular fatty acid levels is essential for the analysis of thermogenic function in cultured primary brown and brite/beige adipocytes. EMBO Reports 15(10):1069–1076.
[41] N'Diaye, E.N., Kajihara, K.K., Hsieh, I., Morisaki, H., Debnath, J., Brown, E.J., 2009. PLIC proteins or ubiquilins regulate autophagy-dependent cell survival during nutrient starvation. EMBO Reports 10(2):173–179.
[42] Mindell, J.A., 2012. Lysosomal acidification mechanisms. Annual Review of Physiology 74:69–86.
[43] Stransky, L.A., Forgac, M., 2015. Amino acid availability modulates vacuolar H+-ATPase assembly. Journal of Biological Chemistry 290(45):27360–27369.
[44] Edwards, N., Anderson, C.M., Gatfield, K.M., Jevons, M.P., Ganapathy, V., Thwaites, D.T., 2011. Amino acid derivatives are substrates or non-transported inhibitors of the amino acid transporter PAT2 (slc36a2). Biochimica et Biophysica Acta 1808(1):260–270.
[45] McGuire, C., Stransky, L., Cotter, K., Forgac, M., 2017. Regulation of V-ATPase activity. Frontiers in Bioscience 22:609–622.
[46] Heublein, S., Kazi, S., Ogmundsdottir, M.H., Attwood, E.V., Kala, S., Boyd, C.A., et al., 2010. Proton-assisted amino-acid transporters are conserved regulators of proliferation and amino-acid-dependent mTORC1 activation. Oncogene 29(28):4068–4079.
[47] Ogmundsdottir, M.H., Heublein, S., Kazi, S., Reynolds, B., Visvalingam, S.M., Shaw, M.K., et al., 2012. Proton-assisted amino acid transporter PAT1 complexes with Rag GTPases and activates TORC1 on late endosomal and lysosomal membranes. PLoS One 7(5):e36616.
[48] Pramme-Steinwachs, I., Jastroch, M., Ussar, S., 2017. Extracellular calcium modulates brown adipocyte differentiation and identity. Scientific Reports 7(1): 8888.
[49] Lee, I.H., Cao, L., Mostoslavsky, R., Lombard, D.B., Liu, J., Bruns, N.E., et al., 2008. A role for the NAD-dependent deacetylase Sirt1 in the regulation of autophagy. Proceedings of the National Academy of Sciences of the United States of America 105(9):3374–3379.
[50] Stern, O., 1919. Uber die abklingungszeit der fluoreszenz. Physikalische Zeitschrift 20:183–188.

